Science, Engineering and Technology Vol. 6, No. 1, pp. 90-97
www.setjournal.com https://doi.org/10.54327/set2026/v6.i1.313

Green Synthesis of Tin Oxide (SnO_2) Nanoparticles from *Senna alata* Leaves Extract

Oludele Adegboyega[1], Israel Adewoye Adegboyega[2], Jacob Adedayo Adedeji[2]

[1]*Department of Physics, Emmanuel Alayande University of Education, Oyo, Oyo State, Nigeria.*

[2] *Sustainable Environment and Transportation Research Group (SET-RG), Department of Civil Engineering Midlands, Durban University of Technology, Pietermaritzburg, 3201, South Africa.*

Abstract

The plant-mediated synthesis of metal oxide nanoparticles is an eco-friendly and sustainable approach for hazardous chemical- and energy-expending protocols. Chemically synthesized methods often use toxic reagents and are biological hazards, whereas physical methods require special equipment and may lead to the loss of control of the particles. In this work, fresh Senna alata leaf extract was used to synthesize SnO_2 nanoparticles via a green route as reducing, stabilizing, and capping agents. A metal precursor (1.0 M tin chloride) was utilized. The prepared nanoparticles were characterized via X-ray diffraction (XRD), Fourier transform infrared (FTIR) spectroscopy, scanning electron microscopy (SEM), transmission electron microscopy (TEM), and ultraviolet–visible (UV–Vis) spectroscopy to investigate their structural, morphological and optical properties. As derived from the XRD measurements, a major peak was detected for the [002] plane, and the average crystallite size was 8.25 nm, with a d-spacing value of approximately 0.2575 Å, corresponding to nanocrystalline SnO_2, which confirmed its successful formation. The FTIR analyses revealed characteristic molecular vibrations related to structures of SnO_2. Scanning and transmission electron microscopic evaluations revealed crystallites with distinctive morphologies of SnO_2 nanoparticles. The absorption edge is approximately 300 nm, and the bandgap energy is estimated to be 4.57 eV via optical characterization. The preferred [002] orientation, nanoscale crystallinity and wide bandgap make the synthesized SnO_2 nanoparticles multifunctional. These properties render them excellent candidates for optoelectronic and environmental sensors, energy storage applications, and anticorrosion coatings, providing a versatile architecture for designing next-generation nanotechnologies.

Keywords*: Green synthesis, Characterization, Tin oxide, Nanoparticles, Senna alata.*

1. Introduction

Metal oxide nanoparticles have emerged as versatile materials for applications in catalysis, sensors, optoelectronic devices, and environmental remediation [1]. Various metal oxide semiconductors have been attempted for this purpose, including titanium dioxide (TiO_2), zinc oxide (ZnO), tin dioxide (SnO_2), strontium titanate ($SrTiO_3$), niobium-pentoxide (Nb_2O_5) and barium stannate ($BaSnO_3$). Among them, SnO_2 has exhibited promising features because of its combined properties [2]. These advantages include excellent transparency in the visible region (since 1991), enormous chemical and physical adsorption of species, thermal stability under air up to 5000 °C, and workability at quite low temperatures. Tin dioxide, with a wide band gap of 3.6–3.8 eV, is an n-type semiconductor that has been widely used in gas sensing, catalysis, transparent conductive films, lithium-ion batteries, optoelectronic devices and environmental cleanup [3].

Corresponding author: Jacob Adedayo Adedeji (jacoba@dut.ac.za)
Received: 26 August 2025; Revised: 12 January 2026; Accepted: 16 January 2026; Published: 6 March 2026

The charge carrier mobility is faster in SnO_2 [4]. SnO_2 photoanodes have undergone substantial advancements since SnO_2 was originally used in DSSCs. These advancements include morphological regulation, doping with diverse species, surface alternations, and hybrid structures with other oxide semiconductors [5]. Vilas et al. [6] successfully synthesized tin oxide (SnO_2) via a microwave-assisted method. The photo conversion efficiency of the DSSC based on the pH variation in SnO_2 was also studied. The DSSC assembled using the SnO_2 photoanode at pH 12 exhibited a higher energy conversion efficiency than the other SnO_2 photoanodes at pH 8, 9, and 10.

SnO_2 and other metal oxide nanoparticles can be prepared via a number of typical methods, such as sol-gel [7], precipitation [8], electrochemical [9], sonochemical [10], solid-state [11], alcohothermal methods or microwave-induced synthesis routes [13]. However, such methods are commonly performed in the presence of toxic organic solvents and reducing agents that may be harmful to both environmental and biological systems. Thus, much attention has been drawn to the design of alternative synthetic methods employing safe, non-toxic, and biocompatible materials in aqueous media [14]. Recently, the biological synthesis of metal oxide NPs via plant extracts has become one of the most promising methods, and it has been reported as a green or sustainable alternative to conventional chemical and physical methods [15], [16], [17], [18]. Plant extracts may act as reducing and stabilizing agents during NP synthesis [19]. This green synthesis technique provides an affordable, scalable and environmentally friendly route to metal/metal oxide nanoparticles.

This research is significant because it offers a low-cost, environmentally sustainable alternative to conventional SnO_2 nanoparticle synthesis routes, which often involve toxic chemicals. By using Senna alata, a widely available medicinal plant, this study introduces a novel and underutilized green resource for nanomaterial synthesis. This study contributes to the growing field of green nanotechnology and supports broader efforts toward safer and more sustainable functional nanomaterials for use in energy, environmental, and electronic applications.

In recent years, researchers have explored the use of plant-based materials for the biosynthesis of metal oxide nanoparticles. Abiodun et al. [20] stressed the importance of incorporating green-synthesized copper oxide nanoparticles into the counter electrode of monolithic dye-sensitized solar cells (MDSSCs) as eco-benign and even dispersing materials, suggesting their potential as promising nanomaterials for DSSC applications. Abiodun et al. [21] reported that the potential of incorporating green-synthesized iron oxide nanoparticles into MDSSC counter electrodes was due to their excellent biocompatibility and even dispersion.

The present work demonstrates the green synthesis of SnO_2 nanoparticles from fresh leaf extract of Senna alata. The extract is rich in many other bioactive phytochemicals that could serve as reducing and stabilizing agents in the formation of nanoparticles. The plant-mediated synthesis approach presented here provides a cost-effective, environmentally friendly alternative to chemical synthesis. The as-prepared SnO_2 nanoparticles have been extensively studied in terms of their structural, morphological and optical characteristics. Analytical tools such as X-ray diffraction (XRD), FT-IR, scanning electron microscopy (SEM), transmission electron microscopy (TEM) and UV–Vis spectroscopy were used for the characterization of the crystals to investigate their crystal orientation, functionalization, surface morphology/particle size distribution and optical absorbance behavior, which were discussed in detail. Therefore, the main aim of this work was to establish the green synthesis of SnO_2 nanoparticles from a fresh Senna alata leaf extract as natural reducing and stabilizing agents and to reveal their optical, structural, morphological properties via different advanced analysis instruments.

2. Materials and Methods

This section describes the materials and experimental procedures used to synthesis and characterize the prepared samples. It gives a structured description of the raw materials, synthesis methodology, and analytical techniques used to ensure that the results are reproducible and reliable.

2.1. Materials

Candlestick plant leaves (*Senna alata*) were harvested from a plant growing on a farm in the Baale Yaku neighbourhood of Ogbomoso, Oyo State, Nigeria.

Distilled water was used as the solvent, while analytical-grade tin chloride was utilized without undergoing additional purification.

2.2. Methods

Fresh Senna alata leaves were obtained from a rural area (a farm in the Baale Yaku neighbourhood of Ogbomoso, Oyo State, Nigeria). The leaves were first rinsed with clean water to remove dust and surface impurities. Distilled water was selected as the solvent for extracting phytochemicals from Senna alata because of its high efficiency in dissolving bioactive compounds. Distilled water is also widely regarded as a safe, effective, and environmentally friendly solvent for plant extraction. The fresh leaves of Senna alata were ground well with an electric blender, and the extract was then filtered through Whatman no. 1 filter paper. The green color extract was obtained and stored in a flask.

A total of 1.0 M tin chloride was dissolved in 100 mL of distilled water in separate beakers and stirred with a magnetic stirrer for 120 s. In a typical procedure, plant extract (Senna alata) leaves in aqueous solution were added dropwise at a ratio of 1:10 to a tin chloride solution [22]. A color change was observed, and the resulting mixtures were then centrifuged with a centrifuge model 800 manufactured via fly change cooling technology and then decanted (the liquid was separated from the solid particles that settled at the bottom of the container). The pellets were then removed from the centrifuge tubes, which were completely dried in an oven at 60 °C for 24 h. The pellets were light yellow in color, which confirmed the synthesis of tin oxide nanoparticles (Figure 1).

2.3. Characterization techniques

X-ray diffraction (XRD) (model: JEOL JBM-7600F) was used to determine the crystallographic structure. The functional groups and component compositions of the nanoparticles were determined via a Cary 630 FTIR spectrometer (Agilent Technology). The surface morphology was determined via SEM (model: Rigaku) and high-resolution TEM (model: Verios 460 l). The optical properties of the SnO_2 nanoparticles were analysed via UV–vis spectroscopy (model: JASCO-V670) in the range of 200–900 nm, and the optical bandgap was estimated from the optical absorption spectrum.

3. Results and Discussion

This section discusses the results obtained from the structural, morphological, and optical analyses of the synthesized SnO_2 nanoparticles. The data are interpreted to establish relationships between the synthesis process and the resulting material properties, and the findings are compared with reported studies to assess consistency and performance.

Figure 1. Synthesis of SnO_2 NP.

Table 1. Structural Parameters of Colloidal SnO_2 Nanoparticles.

Peak	2θ (°)	FWHM	Intensity (a.u)	Sin θ	Cos θ	d (Å)	hkl	L (nm)
1	27.0	1.057	200	0.2334	0.9723	0.33	002	8.08
2	28.0	1.057	100	0.2419	0.9702	0.32	101	8.10
3	36.1	1.057	30	0.3709	0.9205	0.20	200	8.14
4	51.2	1.057	50	0.4320	0.9018	0.18	220	8.68

3.1. Structural characteristics of the synthesized SnO_2 nanoparticles

3.1.1. XRD characterization of the synthesized SnO_2 nanoparticles

X-ray diffraction measurements of the tin oxide nanoparticles were carried out, and the results are shown in Figure 2. The following miller indices, [002], [101], [200] and [220], were assigned diffraction angles of 27.0 °, 28.5 °, 36.1° and 50.4 °, respectively, which confirmed the presence of SnO_2 crystals with tetragonal Romarchite structures. The most prominent SnO_2 peak [002] reflection was observed at a diffraction angle of 2θ = 27.0°, confirming the presence of SnO_2 crystals. Two other dominant diffraction peaks are located at 28.5° and 50.4° and correspond to the crystallographic planes [101] and [220] of the tetragonal Romarchite structure, respectively.

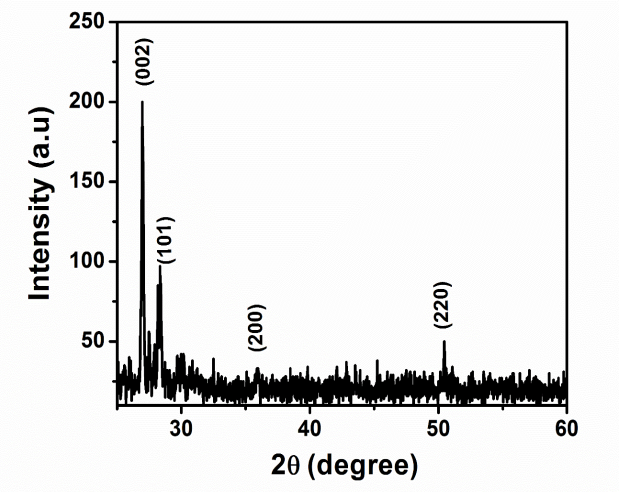

Figure 2. XRD patterns of the SnO2 nanoparticles.

Additionally, a weak SnO_2 diffraction peak is located at 36.1° and corresponds to the crystallographic planes [200]. The X-ray diffraction (XRD) pattern exhibited sharp and well-defined peaks, which were in excellent agreement with the standard JCPDS card no. 41–1445, and was characterized as a symmetric tetragonal rutile-type crystal phase of SnO_2 nanoparticles (romarchite). The peak broadening and relatively low intensity of the observed peaks are indications of nanosized crystallites. The average crystallite size and interplanar spacing (d-spacing) based on the data in Table 1 were computed to be approximately 8.25 nm and 0.2575 Å, respectively. These values are well correlated with the observations from earlier studies [23],]24].

The nanoscale structure and [002] orientation enhance the sensitivity for gas sensing applications. This is in agreement with the work of Miller et al. (2014) [24], who studied nanoscale metal oxide-based heterojunctions for gas sensing. The high surface area and nanostructure make it suitable for heterogeneous catalysis and photocatalysis (e.g., degradation of pollutants under UV light).

3.1.2. FTIR characterization of the synthesized SnO_2 nanoparticles

To determine the structural properties of the SnO_2 nanoparticles prepared from fresh Senna alata leaf extract in aqueous media, Fourier transform infrared (FTIR) spectroscopy was used, and the results are depicted in Figure 3. The FTIR spectrum revealed a number of clear absorption bands corresponding to the functional groups attached to the surface of the nanoparticles. The bond types and wavenumbers in the colloidal SnO_2 nanoparticles are shown in Table 2. The striking peak at 1622.00 cm^{-1} is attributed to the vibration of nitrate anions (NO_3^-). The wide absorption peak at 3482.00 cm^{-1} was assigned to the O–H stretching vibration of either the surface hydroxyl group or adsorbed water [25]. The 1050.00 cm^{-1} band is attributed to the asymmetric vibration of C–O stretching, and the vibration at 2926.00 cm^{-1} indicates –C–H stretching vibrations.

Table 2. Summary of Bond types and Wavenumbers in Colloidal SnO_2 Nanoparticles FTIR Spectrum.

Peak	Wavenumber (cm^{-1})	Bond type
1	3482.00	OH stretch
2	2926.00	C-H stretch
3	1622.00	NO_3^- stretch
4	1050.00	C-O stretch

Several molecular vibration frequencies, including NO_3- (1622.00 cm^{-1}, VNO_3^-), OH (VOH, 3482.00 cm^{-1}), C–O (VC-O, 1050.00 cm^{-1}) and C–H (VC-H, 2926.00 cm^{-1}), are shown in Figure 3. These functional groups are in accordance with the results obtained by [26].

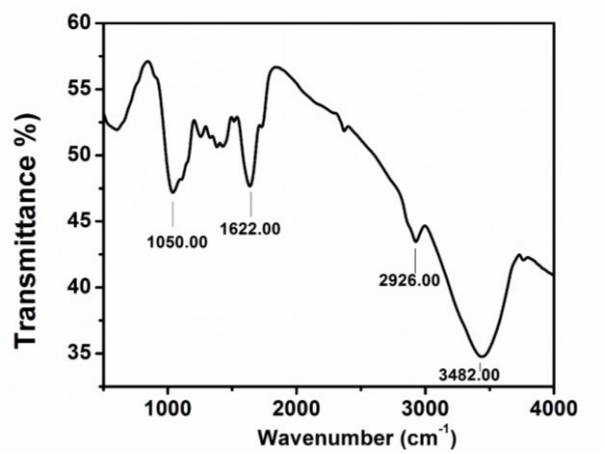

Figure 3. FTIR spectrum of SnO_2 nanoparticles synthesized using fresh *Senna alata* leaves and water as the solvent.

3.2. Morphological characteristics of the synthesized SnO_2 nanoparticles

3.2.1. SEM characterization of synthesized SnO_2 nanoparticles

SEM images of the prepared SnO_2 nanoparticles are shown in Figure 4 at 9000× and 10000× magnifications. The micrographs revealed homogeneous surface coverage with fairly consistent morphology. Most of the nanoparticles are spherical and have good dispersion, with some of them being partially agglomerated into irregular clusters. Individual crystallites can be easily recognized owing to their distinct boundaries and preferential rounding at edges. Under lower magnification (9000×), several microcracks are observed, which indicate poor interparticle adhesion and better surface characteristics [27]. The microscopic mean grain size was determined to be approximately 20 nm on the basis of the intercept procedure. This grain size is larger than the size of crystallites determined via Scherrer's equation, which could be attributed to the agglomeration of smaller crystallites during the formation of nanoparticles.

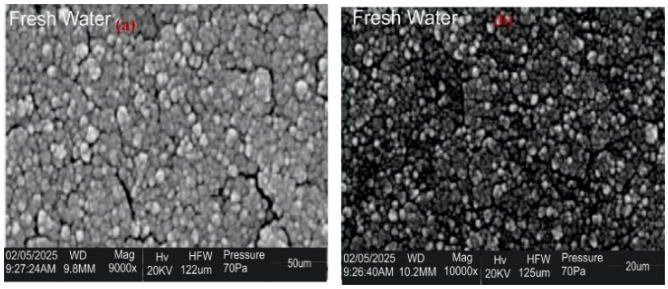

Figure 4. SEM images of synthesized SnO_2 nanoparticles using fresh *Senna alata* leaves and water as the solvent.

3.2.2. TEM characterization of synthesized SnO_2 nanoparticles

TEM images of the prepared SnO_2 nanoparticles are presented in Figure 5, which shows that the particle size varies from 20 nm to 100 nm. By analysing the TEM micrographs, it was possible to carry out a statistical analysis of the grain sizes, and a distribution of well-dispersed (i.e., nonagglomerated) nanoparticles was found with a relatively small dispersion between 9–11 nm. These values match the particle sizes estimated from the XRD pattern well and confirm the coherence of the structural analysis. Moreover, there are some clear lattice fringes in the images, indicating that single-crystalline SnO_2 nanostructures were obtained. The average particle sizes are in good agreement with the values from previous research [28].

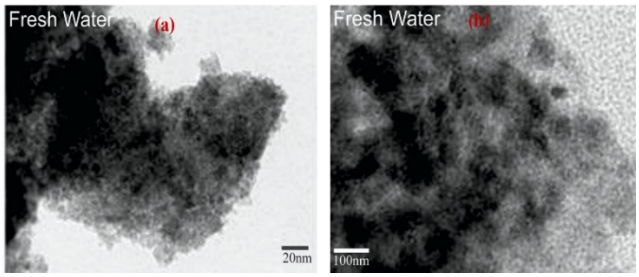

Figure 5. TEM images of synthesized SnO_2 nanoparticles using fresh *Senna alata* leaves and water as the solvent.

3.3. Optical characteristics of tin oxide (SnO_2) nanoparticles

3.3.1. Optical Absorbance Spectra of SnO_2 Nanoparticles

Figure 6 shows an absorbance–wavelength plot of SnO_2 nanoparticles synthesized from fresh *Senna alata* leaves and water as the solvent in the UV–Vis–NIR region, with distinct absorption edges. The SnO_2 nanoparticles absorb UV light, whereas they are transparent in the visible region of the solar spectrum. The absorbance–wavelength plot of the SnO_2 nanoparticles shows maximum absorption at approximately 300 nm. Additionally, the plot reveals two other minor peaks corresponding to 400 nm and 670 nm. The plot also shows that the SnO_2 nanoparticles have a higher absorption coefficient within the UV region of the solar spectrum. Its ability to absorb UV light makes this material suitable for coatings to block or absorb harmful UV radiation (e.g., in windows or protective films).

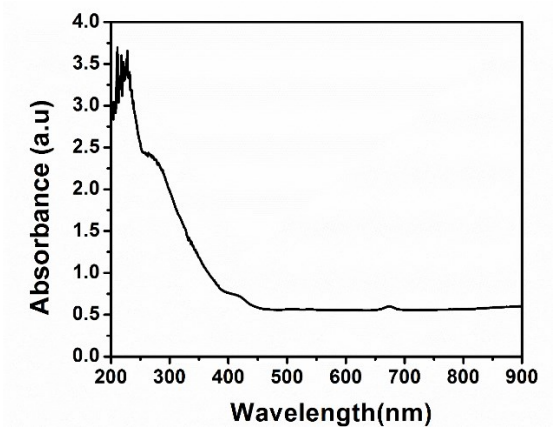

Figure 6. Absorbance–wavelength plot of synthesized SnO_2 nanoparticles using fresh *Senna alata* leaves and water as the solvent.

3.3.2. Optical transmittance spectra of the SnO_2 nanoparticles

The transmittance–wavelength relation shown in Figure 7 clearly shows sigmoidal behavior with the onset of transmittance at approximately 300 nm. Hereafter, the transmittance gradually increases with increasing wavelength in the range of 300–420 nm (UV) due to the strong absorption of UV light by the SnO_2 nanoparticles. Notably, the plot shows slight attenuation peaks at wavelengths of approximately 490 nm, 525 nm, 630 nm and 670 nm. These absorption dips can be related to electronic transitions or retained phytochemicals remaining from the plant-based synthesis, which again adds to the optoelectronic action of the nanomaterial. These slight attenuations were due to the scattering of the absorbed light. This result also corroborates the absorbance results.

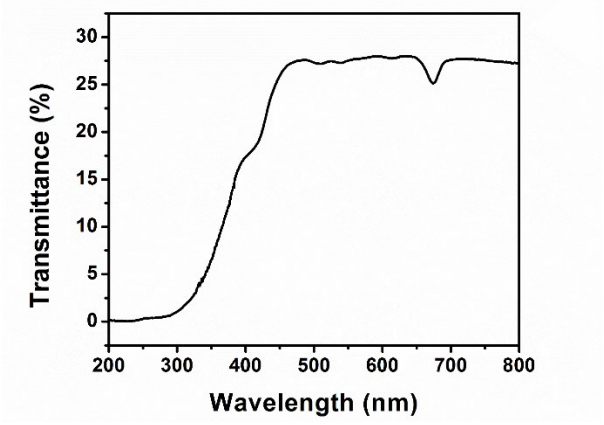

Figure 7. Transmittance–wavelength plot of synthesized SnO_2 nanoparticles using fresh *Senna alata* leaves and water as the solvent.

3.3.3. Optical energy bandgap spectra of SnO_2 nanoparticles

Figure 8 shows the Tauc plot that was used to estimate the optical bandgap of these synthesized SnO_2 nanoparticles from the absorption edge. The absorption coefficient (α) was calculated as the absorbance/film thickness, where h and ν are Planck's constant and the frequency of incident light, respectively. For a direct bandgap semiconductor, i.e., SnO_2 here, the curve of $(\alpha h\nu)^2$ versus the photon energy (hν) should show good linearity, and the extrapolation to the energy axis gives us an estimation of its bandgap value. The estimated bandgap of the synthesized SnO_2 nanoparticles was 4.57 eV. This value is in agreement with the reported literature data for SnO_2 nanomaterials [29] and supports the optical properties of the material. The wide bandgap and absorption edge of 300 nm in the UV range make this material ideal for UV photodetectors or UV light sensors (e.g., solar-blind UV detection, flame sensors, or UV monitoring systems). The wide bandgap enables UV-driven photocatalytic activity for water splitting and organic pollutant degradation. The wide bandgap and high visible transparency make the material a promising candidate for transparent conducting oxide applications in displays, solar cells, and smart windows, with a nanoscale size that enhances optical clarity and conductivity.

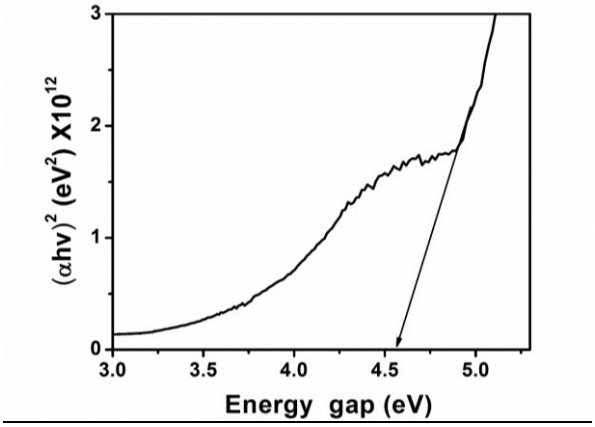

Figure 8. (αhν)2-Energy plot of synthesized SnO_2 nanoparticles using fresh *Senna alata* leaves and water as the solvent.

4. Conclusions

The present work has shown an efficient green protocol for the synthesis of SnO_2 nanoparticles through the aqueous extraction of freshly collected leaves of

Senna alata. Characterization of the synthesized nanoparticles was performed via UV–Vis spectrophotometry, XRD, FTIR spectroscopy, SEM, and TEM. Optical studies revealed that the absorption edge is approximately 300 nm and that the estimated direct band gap is 4.57 eV. XRD also revealed the formation of SnO_2 with a well-defined peak corresponding to the [002] lattice plane, and the FTIR data revealed molecular vibration frequencies typical of SnO_2 architectures. Morphological analyses by SEM and TEM provided additional evidence for the formation of well-crystallized SnO_2 crystallites with a size and shape characteristic of nanoparticles. The results reveal the potential use of plant-mediated synthesis as a green, clean, and low-cost method for the one-phase production of highly crystalline SnO_2-based nanomaterials with excellent optical properties.

The combination of a dominant [002] orientation, nanocrystallinity, and wide optical bandgap imparts multifunctional characteristics to the synthesized SnO_2 nanoparticles. These properties collectively open pathways for applications in optoelectronics, environmental sensing, energy storage, and protective coatings, establishing the material as a versatile platform for future nanotechnology-driven innovations.

Future research could investigate doping these green-synthesized SnO_2 nanoparticles with other metal or nonmetal elements to improve their functional characteristics for specific applications. Investigating their performance in specific devices, such as gas sensors, photocatalysts, or solar cells, would help to validate their practical application. Furthermore, expanding the green synthesis technique and evaluating its repeatability and cost feasibility in commercial settings would be significant.

Competing Interest Statement

The authors declare no known competing financial interests or personal relationships that could have influenced the work reported in this paper.

Data and Materials Accessibility

No data or additional materials were utilized for the research described in the article.

References

[1] C. Aprile, E. Gobechiya, J. A. Martens, and P. P. Pescarmona, "New mesoporous composites of gallia nanoparticles: high-throughput synthesis and catalytic application," *Chem. Commun.*, vol. 46, no. 41, pp. 7712–7714, 2010.

[2] Y. Duan, J. Zheng, N. Fu, Y. Fang, T. Liu, Q. Zhang, X. Zhou, Y. Lin, and F. Pan, "Enhancing the performance of dye-sensitized solar cells: doping SnO_2 photoanodes with Al to simultaneously improve conduction band and electron lifetime," *J. Mater. Chem. A*, vol. 3, pp. 3066–3073, 2015, doi: 10.1039/C4TA05923A.

[3] T. W. Kim, J. K. Kwak, K. H. Park, D. Y. Yun, D. U. Lee, D. I. Son, J. H. Han, and J. Y. Lee, "Microstructural and optical properties of SnO_2 nanoparticles formed by using a solvothermal synthesis method," *J. Korean Phys. Soc.*, vol. 57, no. 6, pp. 1803–1806, 2010.

[4] T. Y. Li, C. Su, S. B. Akula, W. G. Sun, H. M. Chien, and W. R. Li, "New pyridinium ylide dyes for dye sensitized solar cell applications," *Org. Lett.*, vol. 18, pp. 3386–3389, 2016, doi: 10.1021/acs.orglett.6b01539.

[5] G. Shang, J. Wu, M. Huang, J. Lin, Z. Lan, Y. Huang, and L. Fan, "Facile synthesis of mesoporous tin oxide spheres and their applications in dye-sensitized solar cells," *J. Phys. Chem. C*, vol. 116, pp. 20140–20145, 2012, doi: 10.1021/jp304185q.

[6] Y. K. Vilas, S. K. Vishal, V. J. Chaitali, B. C. Nandu, U. M. Ravindra, N. S. Pandit, E. L. Prasad, and M. P. Habib, "Synthesis of tin oxide nanoparticles using microwave-assisted method for dye-sensitized solar cell application," *ES Energy Environ.*, vol. 23, no. 1104, pp. 1–11, 2024.

[7] C. H. Shek, J. K. L. Lai, and G. M. Lin, "Grain growth in nanocrystalline SnO_2 prepared by sol-gel route," *Nanostruct. Mater.*, vol. 11, no. 7, pp. 887–893, 1999.

[8] H. Wang, X. Xu, J. Zhang, and C. Li, "A cost-effective coprecipitation method for synthesizing indium tin oxide nanoparticles without chlorine contamination," vol. 26, no. 11, pp. 1037–1040, 2010.

[9] W. Chen, D. Ghosh, and S. Chen, "Large scale electrochemical synthesis of SnO_2 nanoparticles," *J. Mater. Sci.*, vol. 43, no. 15, pp. 5291–5299, 2008.

[10] D. N. Srivastava, S. Chappel, O. Palchik, A. Zaban, and A. Gedanken, "Sonochemical synthesis of mesoporous tin oxide," *Langmuir*, vol. 18, no. 10, pp. 4160–4164, 2002.

[11] A. R. Sinha, M. Pradhan, S. Sarkar, and T. Pal, "Large-scale solid-state synthesis of Sn-SnO_2 nanoparticles from layered SnO_2 by sunlight: A material for degradation in water by photocatalytic reaction," *Environ. Sci. Technol.*, vol. 47, no. 5, pp. 2339–2345, 2013.

[12] D. F. Zhang, L. D. Sub, G. Xu, and C. H. Yan, "Size-controllable one-dimensional SnO_2 nanocrystal: synthesis growth mechanism, and gas sensing property," *Phys. Chem. Chem. Phys.*, vol. 8, no. 42, pp. 4874–4880, 2006.

[13] F. I. Pires, E. Joanni, R. Sav, M. A. Zaghete, E. Longo, and J. A. Varela, "Microwave-assisted hydrothermal synthesis of nanocrystalline SnO_2 powders," *Mater. Lett.*, 2008.

[14] A. S. Pereira, N. J. Silva, T. Trindade, and S. Pereira, "A single-source route for the synthesis of metal oxide

nanoparticles using vegetable oil solvents," *J. Nanosci. Nanotechnol.*, vol. 12, no. 12, pp. 8963–8968, 2012.

[15] F. T. J. Ngenefeme, J. E. Namanga, N. J. Eko, Y. D. Mbom, N. D. Tantoh, and K. W. M. Rui, "One pot green synthesis and characterization of iron oxide-pectin hybrid nanocomposite," *Open J. Compos. Mater.*, vol. 3, no. 2, pp. 30–37, 2013.

[16] M. Mahdavi, F. Namvar, M. B. Ahmad, and R. Mohamad, "Green biosynthesis and characterization of magnetic iron oxide (Fe_3O_4) nanoparticles using seaweed (Sargassum muticum) aqueous extract," *Molecules*, vol. 18, pp. 5954–5964, 2013.

[17] C. Vidya, S. Hiremath, M. N. Chandraprabha, M. A. L. Antonyraj, I. V. Gopal, A. Jain, and K. Bansal, "Green synthesis of ZnO nanoparticles by Calotropis gigantea," *Int. J. Curr. Eng. Technol.*, Special Issue, pp. 118–120, 2013.

[18] S. Gunalan, R. Sivaraj, and V. Rajendran, "Green synthesis ZnO nanoparticles against bacterial and fungal pathogens," *Prog. Nat. Sci. Mater. Int.*, vol. 22, no. 6, pp. 693–700, 2012.

[19] R. P. Singh, V. K. Shukla, R. S. Yadav, P. K. Sharma, P. K. Singh, and A. C. Pandey, "Biological approach of zinc oxide nanoparticles formation and its characterization," *Adv. Mater. Lett.*, vol. 2, no. 4, pp. 313–317, 2011.

[20] A. J. Abiodun, G. A. Alamu, O. O. Daramola, O. Adedokun, and Y. K. Sanusi, "Green synthesis of copper oxide nanoparticles for improved performance in monolithic dye-sensitized solar cells," *Fountain J. Nat. Appl. Sci.*, vol. 13, no. 2, pp. 23–34, 2024.

[21] A. J. Abiodun, G. A. Alamu, O. Adedokun, O. O. Daramola, and Y. K. Sanusi, "Iron oxide green synthesized nanoparticles for improved performance in monolithic dye-sensitized solar cells," *LAUTECH J. Eng. Technol.*, vol. 18, no. 2, pp. 128–137, 2024.

[22] S. S. Behera, J. K. Patra, K. Pramanik, N. Panda, and H. Thatoi, "Characterization and evaluation of antibacterial activities of chemically synthesized iron oxide nanoparticles," *World J. Nanosci. Eng.*, vol. 2, pp. 196, 2012.

[23] L. M. Cukrov, P. G. McCormick, K. Galatsis, and W. Wlodarski, "Gas sensing properties of nanosized tin oxide synthesized by mechanochemical processing," *Sens. Actuators B Chem.*, vol. 77, pp. 491–495, 2007, doi: 10.1016/S0925-4005(01)00751-1.

[24] D. R. Miller, S. A. Akbar, and P. A. Morris, "Nanoscale metal oxide-based heterojunctions for gas sensing: A review," *Sens. Actuators B Chem.*, vol. 204, pp. 250–272, 2014.

[25] J. Zhang and L. Gao, "Synthesis and characterization of antimony doped tin oxide (ATO) nanoparticles," *Inorg. Chem. Commun.*, vol. 7, pp. 91–93, 2004.

[26] S. Blessi, M.M.L. Sonia, S. Vijayalakshmi, and S. Pauline, "Preparation and characterization of SnO2 nanoparticles by hydrothermal method,'' *Int. J. Chem. Res.*, vol. *6*, pp. 2153–2155, 2014.

[27] M. Saravanakumar, S. Agilan, N. Muthukumarasamy, V. Rukkumani, A. Marusamy, P. Umamaheshwari, and A. Ranjitha, "International Journal of ChemTech Research," *Int. J. ChemTech Res.*, vol. 6, no. 14, pp. 5429–5432, 2014.

[28] A. M. E. S. Raj, C. Mallika, O. M. Sreedharan, and K. S. Nagaraja, "Electrical and humidity sensing properties of tin (IV) oxide–tin (II) molybdate composites," *Mater. Res. Bull.*, vol. 36, pp. 837–845, 2001, doi: 10.1016/S0025-5408(01)00570-0.

[29] P. V. Reddy, S. R. Bayathathagari, and S. V. Reddy, "Synthesis and properties of Al doped SnO_2 nanoparticles," *Int. J. ChemTech Res.*, vol. 6, no. 3, pp. 2168–2170, 2014, doi: 10.1016/j.matpr.2016.04.07